Theor. Appl. Climatol. (2006)
DOI 10.1007/s00704-005-0188-2

Theoretical and Applied Climatology
Printed in Austria

[1] Alfred Wegener Institute for Polar and Marine Research, Bremerhaven, Germany
[2] Institute of Meteorology and Climatology, University of Hannover, Germany

Spectral radiance and sky luminance in Antarctica: a case study

S. Wuttke[1] and **G. Seckmeyer**[2]

With 11 Figures

Received November 17, 2004; revised April 29, 2005; accepted August 30, 2005
Published online March 7, 2006

Summary

Sky luminance and spectral radiance has been characterised at Neumayer, Antarctica for selected situations during the austral summer 2003/04. Luminance has also been measured at Boulder, Colorado, USA in June 2003. The high reflectivity of the surface (albedo) in Antarctica, reaching values up to 100% in the ultraviolet (UV) and visible part of the solar spectrum due to snow cover, modifies the radiation field considerably when compared to mid-latitudes. A dependence of luminance and spectral radiance on solar zenith angle (SZA) and surface albedo has been identified. For snow and cloudless sky, the horizon luminance exceeds the zenith luminance by as much as a factor of 8.2 and 7.6 for a SZA of 86° and 48°, respectively. In contrast, over grass this factor amounts to 4.9 for a SZA of 86° and a factor of only 1.4 for a SZA of 48°. Thus, a snow surface with high albedo can enhance horizon brightening compared to grass by a factor of 1.7 for low sun at a SZA of 86° and by a factor of 5 for high sun at a SZA of 48°. For cloudy cases, zenith luminance and radiance exceed the cloudless value by a factor of 10 due to multiple scattering between the cloud base and high albedo surface. Measurements of spectral radiance show increased horizon brightening for increasing wavelengths and generally confirm the findings for luminance. Good agreement with model results is found for some cases; however there are also large deviations between measured and modelled values especially in the infrared. These deviations can only partly be explained by measurement uncertainties; to completely resolve the differences between model and measurement further studies need to be performed, which will require an improvement of modelling the spectral radiance. From the present study it can be concluded that a change in albedo conditions, which is predicted as a consequence of climate change, will significantly change the radiation conditions in polar regions as well.

1. Introduction

Biological organisms react to changes in surface radiation levels. For photosynthesis, the visible part of the solar spectrum (400 to 780 nm), referred to as photosynthetic active radiation (PAR), plays the most important role (Karsten et al., 1999). The biological effectiveness of incident radiation is maximal in the UVB (280 to 320 nm), but varies for different species. This provides the motivation to conduct spectral measurements of radiation parameters (Seckmeyer, 1997).

Spectral irradiance has been monitored at a number of Antarctic sites for more than a decade now (Bernhard et al., 2004; Takao et al., 1999). Since most biological organisms are not horizontally orientated, the knowledge of spectral radiance would present an advantage over spectral irradiance when assessing the impact of incoming radiation on biological organisms. Further, the fraction of diffuse UVB irradiance from global irradiance and the presence of many biologically sensitive organisms that are only partially

sheltered from the sky hemisphere predicates a further need for sky radiance measurements (Grant et al., 1997a). However, spectral measurements of sky radiance in the Antarctic or the Arctic have not been reported in the scientific literature so far.

Sky radiance distributions have been measured by Grant and Heisler (1997), Grant et al. (1997a) and (1997b) focussed on West Lafayette, Indiana, USA, and utilized broadband sensors sensitive to three wavelength bands (UVB, UVA, and PAR). They measured sky radiance for

- clear sky situations, defined by less than or equal to 10% cloud cover determined by hemispheric sky photographs and aerosol turbidity measurements used as an indicator of the uniformity of sky conditions. Evidence of horizon brightening in the UVA, but not in the UVB, was found. Horizon brightening increased with increasing SZA. Further, a region with reduced radiance opposite the solar disk was found (Grant et al., 1997a).
- translucent overcast skies, defined by a cloud cover of greater than 90% determined by hemispheric sky photographs and the solar disk visible on the photographs. No region of reduced radiance opposite the sun was evident in the translucent overcast distributions as was perceived in the clear sky radiance distributions. Horizon brightening was observed for high SZA (Grant et al., 1997b).
- obscured overcast sky, defined by a complete cloud cover determined by hemispheric sky photographs and a PAR transmittance of less than or equal to 0.25. The results showed the highest sky radiance at the zenith and a decline of radiance towards the horizon (Grant and Heisler, 1997).

In all three studies the authors indicated that sky radiance distribution under higher surface albedo conditions, such as snow cover, may differ from their results since the albedo strongly influences the radiance distribution under all cloud conditions.

One of the few measurements of spectral sky radiance has been conducted by Blumthaler et al. (1996). Measurements at various locations in Europe have been performed to investigate a variety of atmospheric conditions. However, there were a lack of measurements over snow covered surfaces. They found a variation in the spatial distribution of sky radiance in the UVB of only 2, but in the UVA by up to a factor of 10. They further concluded that due to increased scattering, sky radiance measurements in the UVB are more sensitive to aerosol particles as well as tropospheric ozone.

Weihs et al. (2000) have investigated the behaviour of sky radiance distribution under broken cloud conditions. The aim of their work was to quantify the alteration in ground UV radiance, compared with those of cloudless skies, which can occur due to broken cloud conditions. Their results showed that, on average, the maximum enhancement in surface UV was due to the reflection of clouds located at 60° to 75° scattering angle and at a viewing zenith angle lower than 30°. Thus, their result is also valid for zenith sky radiance. Radiances from cloudy sky locations were either higher by up to a factor of 2.5 or lower with minimum values being only 8% of the cloudless radiances.

A recent study by Huber et al. (2004) describes spectral sky radiance measurements over a snow covered surface at an Alpine site. Due to the mountainous surroundings, the ground was inhomogeneously covered by snow. They also compared their experimental data with model results from a one-dimensional radiative transfer model. Relative to the modelled situation with homogeneously snow-covered terrain, diffuse sky radiance over snow-free terrain, is reduced by up to 40%, depending on solar zenith angle. They indicate that diffuse sky radiance measurements in a low aerosol environment are especially valuable for the assessment and validation of radiative transfer models. Thus, diffuse sky radiance measurements at an Antarctic site are especially beneficial in this context. Huber et al. (2004) express the need for additional measurements of spectral diffuse sky radiance to comprehensively validate radiative transfer models.

In order to understand radiation conditions in an Antarctic environment it is vital to gain knowledge about characteristics specific to Antarctica. One major difference compared to other parts of the world is the large glaciated area producing a high surface albedo and affecting incident radiation parameters. Therefore, one aim of this study is to assess the influence of a high surface albedo on incident spectral radiance and sky luminance.

Both sky luminance and spectral radiance have been characterised relative to viewing angle for selected periods. A radiative transfer model is evaluated for spectral radiance in an extended wavelength range (290 to 1050 nm) and for high surface albedo conditions. This case study will provide a basis for the characterisation of directional radiation parameters in an Antarctic environment for specific atmospheric conditions, and will contribute to a further understanding of radiation processes in Antarctica.

2. Methods

Measurements of sky luminance and spectral radiance have been performed at the German Antarctic Neumayer Station situated on the Ekström Ice Shelf on the Weddell Sea at 70°39′ S, 8°15′ W during the austral summer 2003/04. Neumayer is a favourable site to conduct radiation measurements. The majority of the station is located beneath the snow surface. Only during the summer campaign a few containers are set up on the surface for the purpose of accommodating additional scientific and technical staff. Thus, the obstruction of measurements due to large buildings are minimised. Since Neumayer is located on an ice shelf, the surrounding surface is homogeneous i.e., a flat snow covered surface.

2.1 Luminance

Sky luminance is detected by a Skyscanner during all types of weather conditions. However, during periods of spectral radiance measurement, sky luminance could not be detected because the Skyscanner was employed to point the radiance entrance optics to the desired direction. The Skyscanner was specifically developed by Czibula & Grundmann GbR (*http://www.photo-meter.com/*) to be utilized in harsh climates. 150 points evenly distributed across the sky are scanned to measure the sky luminance distribution. A scan of the complete sky takes about 40 seconds and is performed every minute. The opening angle of the entrance optics is 10°, which is equivalent to a solid angle of 0.024 sr. This leads to a 57% coverage of the complete sky. As a quality control measure, during each scan, the zenith luminance is measured six times

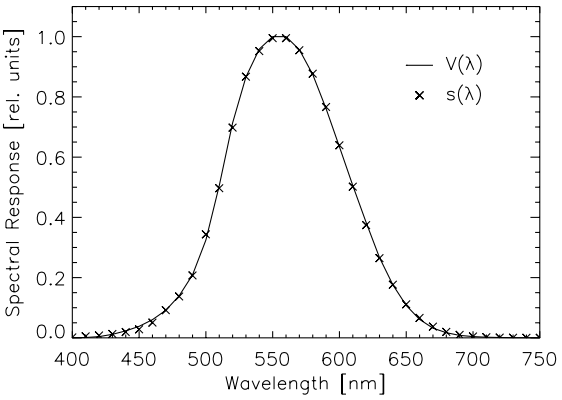

Fig. 1. The response of the luminance sensor $s(\lambda)$ and the response function of the human eye $V(\lambda)$ are shown. Deviations can only be seen around 450 nm where the response is low anyway

(it is expected to stay constant during each scan). For each zenith measurement the azimuth position of the detector is different. Fast moving clouds, for example, can cause a deviation in zenith luminance even within the short period of one scan. Improper levelling of the Skyscanner is another reason for varying zenith luminance. In this case, the centre of the entrance optics is never pointed towards the real zenith.

The response of the luminance sensor $s(\lambda)$ is close to the response of the human eye ($V(\lambda)$). Both responses, $s(\lambda)$ and $V(\lambda)$, are shown in Fig. 1. The luminance sensor itself has been calibrated by Czibula & Grundmann GbR by a standard method for determining luminance. For this procedure a luminance normal and an integrating sphere are used. The inside of this integrating sphere is highly reflective and has a well defined opening through which the radiation reaches the luminance sensor. The opening angle of the luminance sensor is 10°, but the exact value is not relevant for the calibration since it is automatically taken into account by the use of the integrating sphere.

2.2 Spectral radiance

Spectral radiance is detected by pointing a cylindrical input optics to a desired position in the sky with the Skyscanner. The input optics has a field of view (FOV) of 4.4°, which corresponds to $4.63 \cdot 10^{-3}$ sr when integrated. The collected light is led into a Bentham DTMc300 spectroradiometer, which is described in detail by Wuttke

et al. (2005). Similar instruments have been used in UV monitoring at various sites and represent state-of-the-art instrumentation (Bernhard and Seckmeyer, 1999; Bais et al., 2001).

2.2.1 Data collection

The periods of spectral radiance measurements have been determined based on model calculations performed prior to the campaign. The viewing direction opposite the sun (solar azimuth angle + 180°) has been found to be most interesting because the variation of radiance for different viewing zenith angles (VZA) was maximal during cloud free cases. Cloudless situations have also been favoured with respect to the planned model evaluation. To account for the influence of cloud cover, zenith radiance has been measured for both overcast and cloudless sky. Two different data collection protocols have been developed and applied:

1. Zenith radiance has been measured from 280 to 500 nm in steps of 0.25 nm and from 501 to 1050 nm in steps of 1 nm to cover the complete spectrum in a fine wavelength resolution. These fine wavelength steps are necessary for oversampling, which is recommended by Seckmeyer et al. (2001) and in the estimation of possible wavelength shifts. However, it takes around 40 minutes to scan such a spectrum, therefore the wavelength regions have been restricted in the next data collection protocol.
2. Zenithal scans of radiance have been performed in limited wavelength regions. A zenithal scan is defined by a constant viewing azimuth angle (VAA) and varying viewing zenith angles (VZA). In most cases, radiance was detected from the zenith to the horizon in steps of 10°. The preferred VAA was opposite the sun (SAA + 180°), thus in the backward scattering part of the principal plane. The principal plane denotes the plane of the azimuth of the sun, passing through the zenith and back down to the horizon at SAA + 180°. Only limited wavelength regions have been chosen in order to minimise the scan time for one spectrum. To account for various spectral ranges the following wavelength intervals have been sampled: 304 to 306 nm (UVB), 319 to 321 nm (boundary between UVB and UVA), 349 to 351 nm (UVA), 399 to 401 nm (boundary between UVA and visible), and 498 to 500 nm (visible with photomultiplier) in steps of 0.25 nm; 691 to 699 nm (visible with silica diode), 796 to 804 nm (boundary between visible and IR), and 996 to 1004 nm (IR) in steps of 1 nm.

2.2.2 Absolute radiance calibration

Absolute radiance calibration is based on measurements of a 100 W tungsten halogen calibration lamp performed at Neumayer for each day radiance measurements were taken, as well as on 100 W lamp measurements performed in the IMUK radiation laboratory. This 100 W standard was calibrated by Gigahertz Optik GmbH (*http://www.gigahertz-optik.com/*) against lamps calibrated at the German Physikalisch-Technische Bundesanstalt (PTB). Gigahertz Optik maintains a PTB-accredited calibration laboratory. The calibration accuracy of the 100 W standard was additionally verified by comparing the lamp against two independent 1000 W standards from PTB. The deviation between the 100 W lamp and the two 1000 W standards was less than 3% above 300 nm and was relatively independent of wavelength (see *http://lap.phys.auth.gr/qasume/Progress.asp?typeId=2*). This difference is within the typical calibration uncertainty of 3.5% that applies to lamps disseminated by standard laboratories (Bernhard and Seckmeyer, 1999; Kiedron et al., 1999).

The 100 W lamp measurements performed at Neumayer serve to gain knowledge regarding possible changes in the spectroradiometer's responsivity over time. During the Antarctic campaign, the calibration lamp has been deployed inside a portable field calibrator to perform the radiance calibration and stability tests. In order to absolutely calibrate the spectroradiometer for radiance, the complete bulb of the lamp has to be in the field of view of the entrance optics. The distance between lamp and entrance optics in the field calibrator (40 cm) is too short for the lamp to be completely in its field of view. Therefore, it was necessary to measure the 100 W calibration lamp at different distances in the laboratory after the campaign. Furthermore, the radiometric inverse square law (DIN 5031, 1982) had to be verified. It is not trivial that the input cylinder

responds according to this law as the illumination of the entrance slit of the monochromator is not necessarily homogeneous. However, the measurements showed that the inverse square law is fulfilled for distances between 95 and 175 cm within 3%. The 100 W lamp has additionally been measured at a distance of 141.5 cm. Then the irradiance of the lamp was transferred to this distance. The spectral responsivity of the instrument can be described according to Eq. (1):

$$r(\lambda) = \frac{S_L(\lambda)}{E_L(\lambda)}. \quad (1)$$

$S_L(\lambda)$ is the signal of the spectroradiometer when measuring the lamp, and $E_L(\lambda)$ is the spectral irradiance of the lamp as stated in the calibration certificate. With $S_M(\lambda)$ being the signal when measuring the sky, the sprectral irradiance is

$$E(\lambda) = \frac{S_M(\lambda)}{r(\lambda)}. \quad (2)$$

To obtain the absolute spectral radiance a divison by the value of the FOV in sr is necessary. This method of absolute radiance calibration has been applied previously, for example, by Blumthaler et al. (1996). Other methods have been applied which use a calibrated reflectance plaque (see Meister et al., 2003; Mueller et al., 2003). However, most results and conclusions of this study are not based on the absolute value of radiance, but on relative radiance distributions. Despite its higher absolute uncertainty it is therefore justified to use this method.

On the day when the 100 W lamp was measured at large distances in the IMUK radiation laboratory, it has also been measured in the portable field calibrator. This way, the calibration lamp measurements performed at Neumayer have been linked to those performed on the calibration day.

The largest factor that contributes to the overall calibration uncertainty is the uncertainty in the field of view (FOV), which is estimated to $\pm 7\%$. This value is a consequence of the scale reading precision of 0.25° when turning the entrance optics. The calibration certificate of the 100 W lamp is given in wavelength steps of 5 nm. The values were interpolated to intermediate wavelengths with natural cubic splines; the associated uncertainty is 0.2%. The 100 W secondary standard was calibrated at a distance of 50 cm whilst for radiance calibration the irradiance was to be transferred to a distance of 141.5 cm. The inverse square law (Bernhard and Seckmeyer, 1999, 1997) is applied to scale the irradiance values from a distance of 50 cm to 141.5 cm and has an uncertainty of $\pm 3\%$. The uncertainty caused by alignment errors of the lamps and the entrance optics are about 0.1%. Although a high quality current source is used, the precision of the current setting is limited to $\pm 0.01\%$, resulting in an irradiance uncertainty of approximately 0.1% at 300 nm. Consecutive lamp measurements show a reproducibility of about 2%. Together with the uncertainty based on the transfer of the absolute irradiance scale of 3% (see first paragraph in this subsection), the combined uncertainty of these main sources of calibration uncertainty, as defined by Bernhard and Seckmeyer (1999), is 8.4% at 300 nm.

3. Results and discussion

3.1 Luminance

3.1.1 Cloudless vs. cloudy luminance

Two different sky luminance distributions are shown in Fig. 2, for a cloudless and an overcast sky situation in the upper and lower panel, respectively. Since it takes less than a minute to record one scan of sky luminance distribution, Fig. 2 represents an almost instantaneous picture of the sky. The sky dome is projected onto a plane. The absolute luminance is meant to resemble a three dimensional picture. The zenith is in the centre of the projection and the horizon is at the edge. The geographical directions are indicated by N (north), S (south), W (west), and O (east). The grey dot represents the position of the sun in the sky.

The cloudless luminance distribution shown in the upper panel of Fig. 2 was measured on 12 December 2003 at 13:02 UTC (SZA = 47.9°). A rim at the horizon with higher values around $1.36 \cdot 10^4\,\mathrm{cdm}^{-2}$ can be observed. In contrast, the luminance at the zenith (black dot in the upper panel) only reaches $1.8 \cdot 10^3\,\mathrm{cdm}^{-2}$. This feature is called horizon brightening and is also observed in the measurements of spectral sky radiance (see Section 3.2). The maximum luminance with $4 \cdot 10^4\,\mathrm{cdm}^{-2}$ occurs in the aureole, which

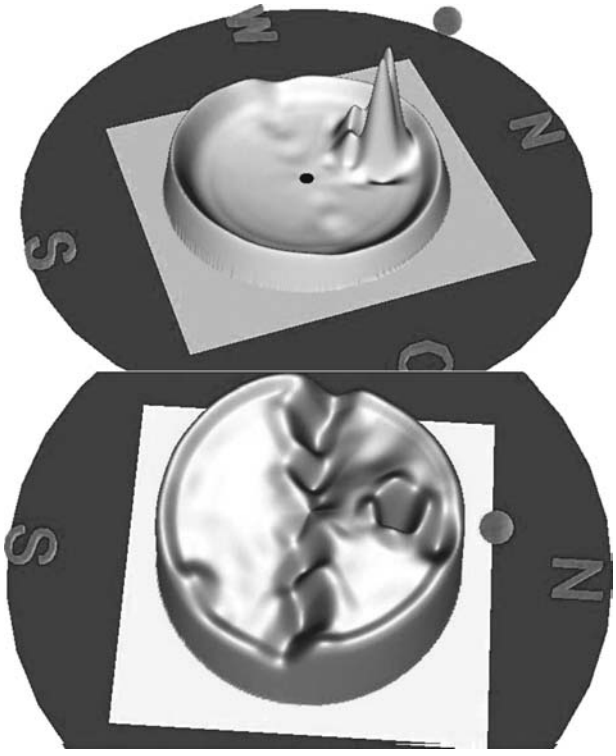

Fig. 2. Sky luminance distribution for a cloudless situation measured on 12 December 2003 at 13:02 UTC (upper panel) and an overcast situation measured on 2 January 2004 at 12:20 UTC (lower panel). Geographical directions are indicated by N (north), S (south), O (east), and W (west). The grey spot represents the sun in the sky. Upper panel: Horizon brightening can be recognised. The maximum luminance occurs in a circumsolar ring around the sun (aureole). Lower panel: Except for the local minimum stretching in east–west direction and the rim at the horizon, the sky luminance distribution is quite uniform

describes the circum-solar region. This maximum occurs because of single scattering in the forward peak of the aerosol scattering phase function (Lenoble, 1993). Aerosols in the periphery of Antarctica are advected by long range transport from their source region in the surrounding Southern Ocean (Piel, 2004).

The feature observed in the aureole, with two major and two minor maxima, is an artefact of the scanning procedure. The sun is not always in the centre of the scanning points surrounding it and therefore the distance between the scan directions surrounding the sun are not equal. As a consequence, the measured luminance surrounding the sun shows varying absolute values. The measurements of sky luminance are reliable at an angular distance of 12° from the sun, which is fulfilled for most solar positions. The small local luminance minimum close to the aureole (see Fig. 2) is not described in the scientific literature and a possible reason for this has not been found.

As the direct luminance of the sun is not measured as it is four to five orders of magnitude higher than the sky luminance and the luminance detector is not designed to cover such a large dynamic range. When the sky luminance entrance optics is directed towards the sun, a shutter prevents the strong direct radiation from entering the system.

The overcast sky shows a different distribution of luminance (see lower panel). This situation was measured on 2 January 2004 at 12:20 UTC (SZA = 47.8°). The distribution of sky luminance is comparably uniform. The luminance at the zenith hardly deviates from the luminance at the horizon reaching values of $1.85 \cdot 10^4\,\mathrm{cdm}^{-2}$ and $1.74 \cdot 10^4\,\mathrm{cdm}^{-2}$, respectively. A local minimum with absolute luminances of roughly 65% of the average luminance stretches from east to west for all VZA. When the upper panel of Fig. 2 is observed closely, a slight minimum in the east–west direction can also be observed. This is not seen as clearly in the cloud free case due to the lower absolute values of diffuse sky luminance.

Up to now, no explanation for this characteristic has been found. Initially it was thought that the weather protection container housing the instruments was responsible for a lower luminance. Due to its blue colour less radiation is reflected from the container compared to the snow surface surrounding it. The influence of the container was tested by rotating the Skyscanner by 90°. After rotation, the local minimum was observed in a north–south direction. Thus, the container cannot be responsible for the reduced luminance. Discussions with the manufacturer have not led to a solution to this problem thus far. Currently, it is assumed that the Skyscanner itself interferes with the measurements. The order in which the different directions are measured is calculated for each scan by a method developed by Tregenza (1987), which mainly depends on SZA. A systematic behaviour combining the order of scan points and the occurrence of the local minimum cannot be observed. Detailed experiments have to be performed in order to investigate this effect.

To further show the difference in absolute values of sky luminance, the diurnal cycle of

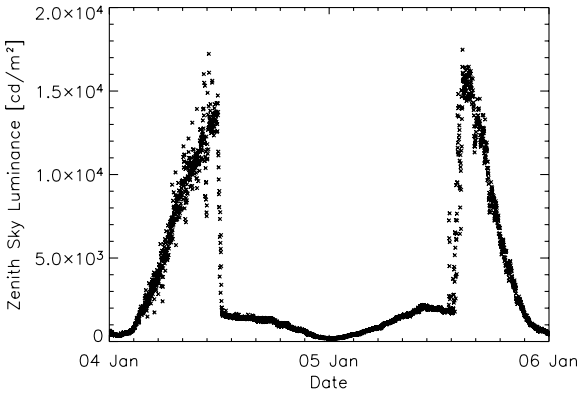

Fig. 3. Diurnal cycle of zenith luminance on 4 and 5 January 2004. The sky was cloud free from midday 4 to midday 5 January. The zenith luminance is lower by one order of magnitude during cloudless sky conditions

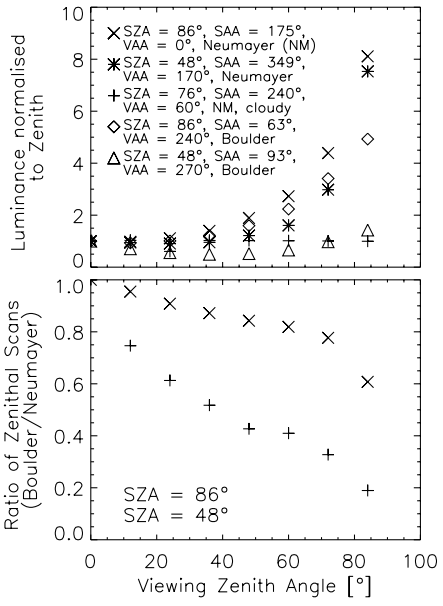

Fig. 4. Upper Panel: Three zenithal scans measured at Neumayer (snow surface) and two measured at Boulder (grass). Horizon brightening can be observed for the cloudless cases over snow, over grass only with a SZA of 86°. Radiance under an overcast sky only varies by ±50%. Lower panel: Ratios of zenithal luminance scans (Boulder/Neumayer) for two SZA. Both ratios are lower than unity and decrease for increasing viewing zenith angle. This implies a stronger horizon brightening for a high albedo surface compared to a low albedo surface

zenith luminance for 4 and 5 January 2004 is plotted in Fig. 3. Both, cloud free and overcast situations occurred. A stratiform cloud cover of eight octas prevailed until noon of 4 January. The sky remained cloudless until noon of the next day, then another stratiform cloud cover moved in. The zenith luminance during both overcast situations reaches $1.7 \cdot 10^4\,\mathrm{cdm}^{-2}$, whereas it stays low with $1.5 \cdot 10^3\,\mathrm{cdm}^{-2}$ for the cloudless situation. In this case, the cloudy zenith luminance is about one order of magnitude higher than the zenith luminance observed in cloud free conditions. This is can be explained by the dominant Mie scattering (Lenoble, 1993) based on the presence of cloud droplets. Incident radiation is attenuated by the cloud droplets which scatter the radiation in any direction. Some photons are scattered out of the clouds and some undergo multiple scattering events before they leave the cloud. In this way, a quite uniform distribution of sky luminance for all VZA is observed during overcast conditions.

3.1.2 Zenithal scans of luminance

Five zenithal scans in the principal plane are depicted in Fig. 4. The luminance is normalised to the zenith luminance. Two cloudless cases measured at Neumayer on 11 and 12 December 2003 with a SZA of 86° and 48°, respectively, and one overcast situation (5 January 2004, SZA = 76°) are shown. The situation for 12 December 2003 is already shown in Fig. 2. Horizon brightening can only be observed for the cloudless zenithal scans. For a SZA of 86°, the luminance at a viewing zenith angle of 84° exceeds the zenith luminance by a factor of 8.2. Horizon brightening is slightly lower for a SZA of 48° with 7.6. For the situation with a stratiform cloud cover, the luminance only varies to ±50%. To assess the influence of the surface albedo, two zenithal scans for a cloud free situation measured at Boulder, Colorado, USA, on 22 June 2003, are also shown. The solar zenith angles are the same as those of the zenithal scans measured at Neumayer (86° and 48°). Horizon brightening is clearly observed for a SZA of 86° reaching a factor of 5. At a SZA of 48°, the luminance at a viewing zenith angle of 84° only exceeds the zenith luminance by a factor of 1.7.

Radiation originating from the horizon has the longest path trough the atmosphere compared to all other viewing directions, thus multiple scattering occurs more frequently. This is the cause for the enhanced luminance observed close to the horizon in comparison with smaller viewing zenith angles.

Horizon brightening is stronger for larger SZA. The path of the direct beam through the atmosphere is very long for large SZA. Attenuation of the direct beam due to scattering is more likely with increasing SZA. Diffuse radiation is therefore, dominant at large SZA. Together with the increased possibility of multiple scattering for increasing viewing zenith angles, the enhanced horizon brightening for large SZA is explained.

The high albedo of the snow surface further enhances the horizon brightening compared to a low albedo surface, such as grass. This is, for example, shown in the upper panel in Fig. 4, where zenithal scans of normalised luminance measured at Boulder and Neumayer are shown. To compare the zenithal scans of normalised luminance measured over grass (Boulder) and snow (Neumayer), the Boulder/Neumayer ratio is shown in the lower panel in Fig. 4, for a SZA of 86° and 48°. Both ratios are below unity and decrease with increasing VZA. The ratio with a SZA of 86° deviates less from unity than the ratio at a SZA of 48°. Two questions arise:

1. Why does the high albedo of the snow covered surface enhance horizon brightening when compared to a low albedo surface?

   Due to the high snow albedo that reaches values up to 1 at 550 nm (Wuttke et al., 2005a) almost all incident radiation is reflected. Backscattering of radiation from atmospheric molecules occurs due to Rayleigh scattering. The longer the path of the radiation through the atmosphere, the more reflection and backscattering occurs. In contrast, for a low albedo surface such as grass with an albedo of 0.09 at 550 nm (Feister and Grewe, 1995), the incoming radiation is almost completely absorbed by the surface. This prevents reflection and in turn backscattering.

2. Why is the enhancement in horizon brightening due to a high albedo surface larger for smaller SZA?

   Due to the shorter path through the atmosphere, the direct beam for low SZA is not attenuated as strongly as for high SZA. Therefore, the fraction of diffuse radiation on global irradiance is less for lower SZA compared to high SZA. For UV wavelengths at different SZA the ratio of direct/global irradiance is shown by Mayer et al. (1997). In the case of an albedo of 0.09 (grass), the reflection of incident radiation at the surface is very small. Therefore, the diffuse component of the global irradiance remains low at low SZA. In contrast, the highly reflective snow covered surface with an albedo of unity also allows reflection of the incident direct irradiance at low SZA. This facilitates backscattering by the atmosphere and leads to an enhancement of diffuse radiation compared to a surface with low albedo.

   At high SZA the path of the direct beam is long and scattering events are more likely to occur before the photons reach the surface. Therefore, horizon brightening can also be observed for low albedo surfaces. However, the effect of horizon brightening is larger with increasing albedo.

Since these luminance measurements have been performed at different locations, parameters influencing the radiative transfer (e.g. aerosols, ozone column, altitude) are not alike. In addition, the Rocky Mountains rise to the west of the measuring site at Boulder. It is most probable that an unobscured view of the horizon at a VZA of 84° is not guaranteed when measuring luminance westwards. In spite of these constraints, it has been shown that for these specific cases, horizon brightening is enhanced over a highly reflective surface. For the investigated cases, horizon brightening is higher by a factor of 5 and 1.7 for a SZA of 48° and 86°, respectively, thus being more pronounced for decreasing SZA.

3.2 Spectral radiance

Diffuse sky radiance has also been measured during the Antarctic campaign to investigate the wavelength dependence on the directional distribution of the diffuse sky radiation.

3.2.1 Cloudless vs. overcast zenith radiance

In Fig. 5, a cloudless and a cloudy spectrum of zenith radiance is shown (upper panel: linear scale, lower panel: logarithmic scale). Both spectra are measured around noon, thus both SZA are roughly the same (47.7° on 19 December 2003, cloudy; 51.2° on 22 January 04, cloudless). At 500 nm, for example, the cloudy spectrum reaches

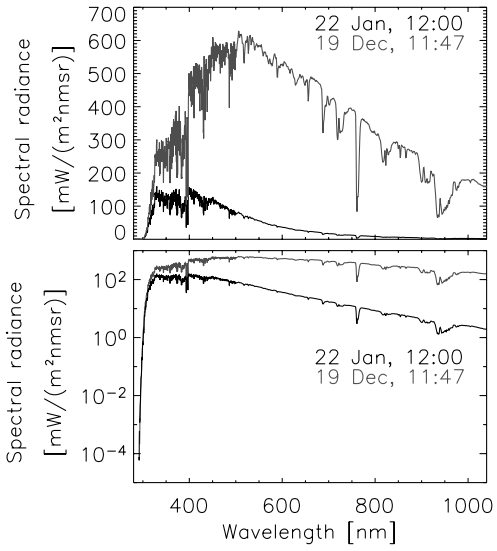

Fig. 5. Cloudless (22 Jan.) and cloudy (19 Dec.) spectrum of zenith radiance. The upper panel shows the spectra on a linear scale, the lower panel on a logarithmic scale. The overcast spectrum exceeds the cloud free spectrum by up to a factor of 10. In addition, the wavelength with maximum radiance is shifted from the UV for the cloudless case to the visible for the overcast situation

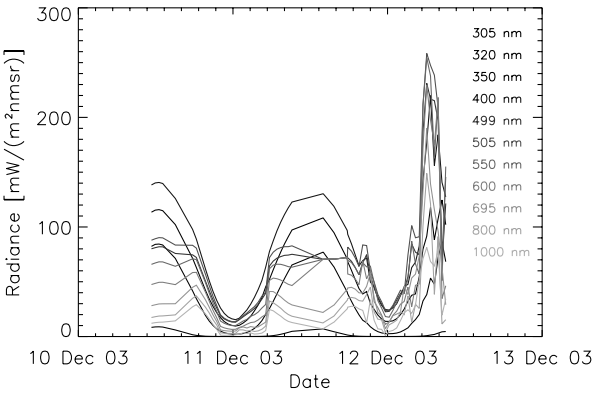

Fig. 6. Diurnal cycle of zenith radiance from 10 to 13 December 2003 for various wavelengths as indicated in the legend. A homogeneous cloud cover was present from 12 December 19:30 UTC. Up to then cloud free conditions prevailed. Zenith radiance for the cloudy situation is much higher compared to the cloudless case

620 m Wm^{-2} nm^{-1} sr^{-1}. At the same wavelength, the cloudless spectrum only shows a value of 80 m Wm^{-2} nm^{-1} sr^{-1}. Looking at the lower panel of Fig. 5, it can be seen that the cloud free spectrum decreases with increasing wavelength by approximately two orders of magnitude. The cloudy spectrum, in contrast, only shows a very slight decrease. The maximum value of the cloudless spectrum is at 400 nm and at about 510 nm for the cloudy spectrum (see upper panel in Fig. 5).

The shape of the two radiance spectra recorded for varying sky conditions can be explained by scattering processes. In a cloudless situation atmospheric Rayleigh scattering is dominant. The strong dependence of Rayleigh scattering on wavelength (Lenoble, 1993) leads to the steep decrease in spectral radiance with increasing wavelength. For cloudy situations Mie scattering at cloud droplets becomes the major process. Mie scattering is hardly dependent on wavelength (Lenoble, 1993) and therefore, the spectral radiance hardly decreases with increasing wavelength.

The shift of maximum radiance from 330 to 510 nm for cloudless and overcast situations, respectively, is also due to enhanced Mie scattering during cloudy situations in combination with the high surface albedo.

The diurnal cycle of zenith radiance for various wavelengths for the period from 10 to 13 December 2003 is shown in Fig. 6. The sky was cloudless up to 19:30 UTC on 12 December. Local maxima can be observed around 06:00 as well as 18:30 UTC for wavelengths larger than 499 nm. This feature may be based on internal reflections inside the input optics. This feature is discussed in detail in Section 3.4.2. During the cloud free periods, the radiance at 400 nm is maximal. As soon as stratiform cloud cover moved in (morning hours of 12 December 2003) the zenith radiance increased.

The higher absolute radiance of the overcast compared to the cloud free radiance spectra is due to multiple reflections between the surface and the clouds. Enhancements in absolute irradiance levels due to a high surface albedo in combination with cloud cover have been observed before (Kylling et al., 2000; Nichol et al., 2003), however, not explicitly for radiance. The effect of snow cover on radiance has been investigated by Huber et al. (2004), and the effect of clouds by Weihs et al. (2000). Both are case studies covering a limited range of atmospheric and surface conditions. The combined effect of clouds and albedo on spectral radiance has not yet been reported in the scientific literature.

3.2.2 Zenithal scans of radiance

Figure 7 shows zenithal scans of radiance for different wavelengths measured at Neumayer during

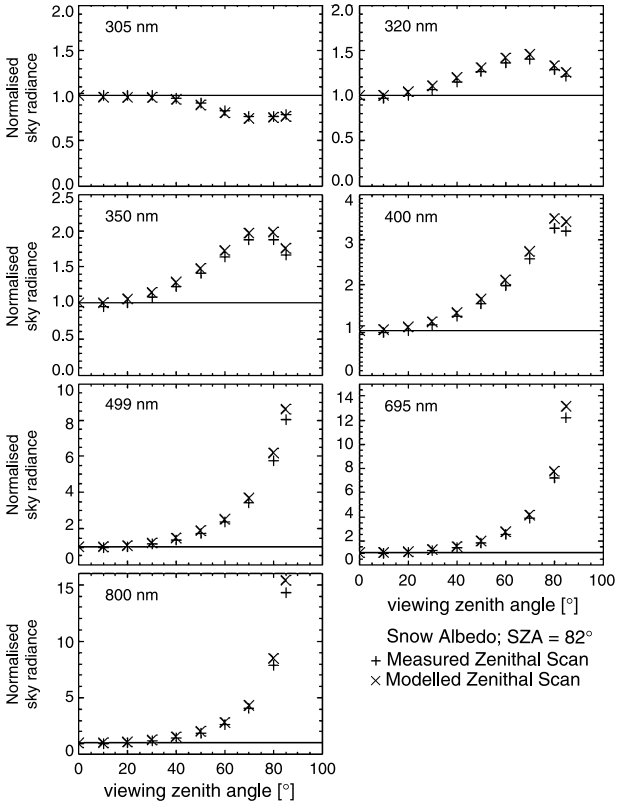

Fig. 7. Measured and modelled zenithal scans of radiance for different wavelengths. Zenithal scans of radiance have been measured over a snow surface and high SZA (82°) in Antarctica. The modelled radiance is slightly higher, especially for large viewing zenith angles. Horizon brightening is seen for all wavelengths in the visible. In the UV, the maximum radiance occurs for different viewing zenith angles

the evening of 9 February 2004, thus with high SZA. The zenithal scan was measured in the principal plane opposite the sun (SAA + 180°) under a cloudless sky. In addition, this situation has been modelled, which is also shown. Measured as well as modelled radiance has been normalised to the zenith. For the model calculations the freely available library for radiative transfer calculations libRadtran (Mayer and Kylling, 2005) has been used. The following most important input parameters include:

Extraterrestial spectrum. Depending on the modelled wavelength either the atlas_plus_modtran or the kurudz_1.0 nm (Kurudz, 1992) extraterrestial spectrum has been used. Atlas_plus_modtran is a combination of Atlas 3 (200–407.8 nm), Atlas 2 (407.8–419.9 nm) and Modtran 3.5 (419.9–800 nm) (Mayer and Kylling, 2005).

Total ozone column. The total ozone column was taken from freely available data from the Total Ozone Mapping Spectrometer (TOMS), which can be obtained from *http://toms.gsfc.nasa.gov/ep_toms/epovplist_l.html*.

Snow albedo. The albedo of snow was taken from albedo measurements performed at Neumayer during the austral summer 2003/04 (Wuttke et al., 2005a).

Radiative transfer solver. For SZA < 80° the radiative transfer solver disort2 has been used, which is a discrete ordinates radiative transfer programme for a multi-layered plane-parallel medium. It was originally developed by Stamnes et al. (1988). For SZA > 80° the radiative transfer solver sdiort has been used. This solver has been developed by Dahlback and Stamnes (1991). It is a pseudo-spherical discrete ordinate method using double precision values.

Aerosols. Aerosols have not been included in the radiative transfer calculations because background aerosol is low in Antarctica. The assumption of neglecting aerosols in Antarctic radiative transfer calculations has also been applied by Bernhard et al. (2004).

In general, horizon brightening increases with increasing wavelength. At short wavelengths in the UVB multiple scattering of diffuse irradiance occurs uniformly across the sky due to the strong wavelength dependence of Rayleigh scattering (Lenoble, 1993). For radiation with long wavelengths, multiple scattering can only be produced by longer paths through the atmosphere, which is the case for directions close to the horizon. Therefore, inhomogeneous radiance distributions are better seen the longer the wavelength.

In order to assess the influence of a snow surface compared to a grass surface, zenithal scans of radiance at different wavelengths have been modelled for a varying surface albedo (see Fig. 8). The zenithal scan over a snow covered surface with a high SZA of 82° represents the situation on 9 February 2004 around 20:15 UTC, which has also been measured (see Fig. 7). The two cases representing the radiance over a grass surface only differ in input albedo, which has been taken from Feister and Grewe (1995). In addition, both albedo situations have been modelled for a low SZA of 48°. The input albedo for snow and grass depending on wavelength is shown in Table 1.

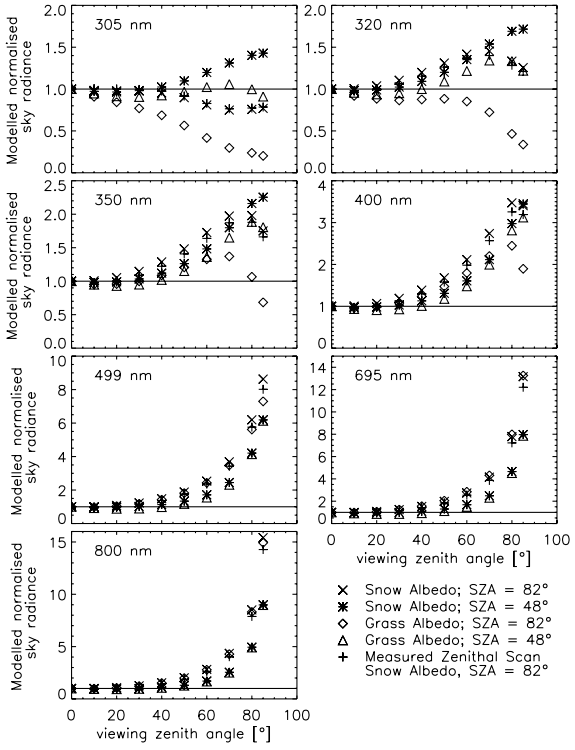

Fig. 8. Modelled zenithal scans of radiance for a high SZA of 82° and a low SZA of 48° over grass and a snow covered surface. For all cases, horizon brightening is seen for all wavelengths in the visible. In the UV, horizon brightening is only observed for the case with snow albedo and SZA of 82°

Table 1. Albedo of snow and grass for different wavelengths. The albedo of grass is taken from Feister and Grewe (1995) and the albedo of snow was measured at Neumayer on 4 January 2004

Wavelength [nm]	Albedo of grass	Albedo of snow
305	0.017	0.971
320	0.017	0.961
350	0.018	0.966
400	0.022	0.967
499	0.035	0.965
550	0.089	0.962
695	0.040	0.900
800	0.587	0.830

UV. For all UV wavelengths, horizon brightening is observed for the case with snow albedo and SZA of 48°. At 400 nm, radiance with a VZA of 86° exceeds the zenith radiance by a factor of 3.5. For grass albedo and SZA of 82° the radiance decreases for increasing VZA for 305 and 320 nm. At 350 and 400 nm, the radiance increases up to a VZA of 70°, and then decreases again. This maximal radiance at a VZA between 70° and 80° is also observed for the grass albedo at a SZA of 48° at 305, 320 and 350 nm as well as for the snow albedo and a SZA of 82° at 320, 350 and 400 nm.

Visible. Horizon brightening is observed for all cases. For both surface types, it is larger with increasing SZA. Maximum horizon brightening is observed over a snow surface at 800 nm with a factor of 15.5 for a SZA of 82°. At 695 nm and a SZA of 82°, horizon brightening for grass is slightly higher than for snow. At a SZA of 48° horizon brightening does not show a strong dependence on the type of surface.

For a closer assessment of the influence of the different types of surfaces, the ratio of the zenithal scans is calculated for a SZA of 82° and 48° (see Fig. 9). The viewing zenith angle is opposite the sun. Most of the ratios remain below unity, which means that the radiance is enhanced

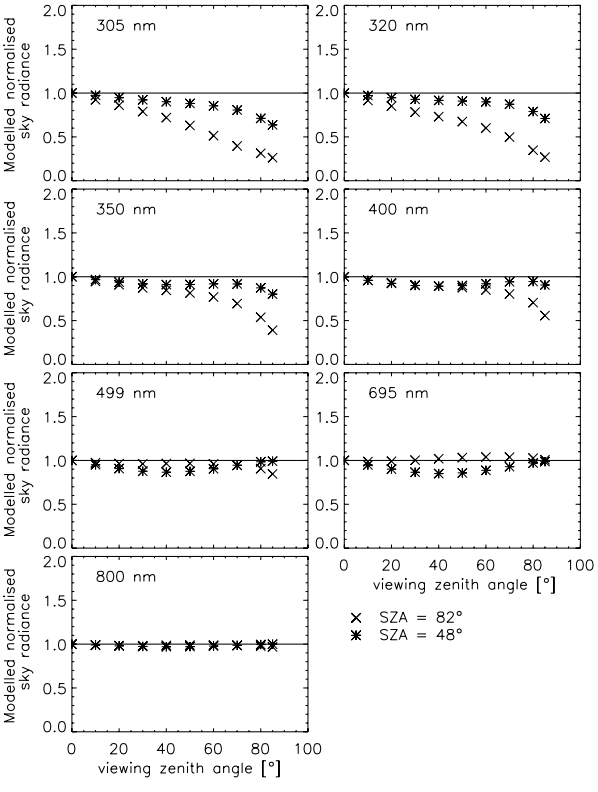

Fig. 9. Modelled ratio of zenithal radiance scans for a SZA of 82° and 48° over a grass and snow surface. At an SZA of 48°, the ratio remains below unity for all wavelengths. This means that radiance over a highly reflective surface is enhanced compared to a surface with a lower albedo. For a SZA of 82°, the ratio is only below unity for 305 and 320 nm. For more details, see text

due to a highly reflective surface in comparison with a low albedo surface. This issue has already been discussed in Section 3.1.2. To explain the spectral differences in the ratio of zenithal scans of radiance, the UV and the visible wavelength ranges are considered separately:

UV. The enhancement due to a high surface albedo is more evident the shorter the wavelength. The reason is the strong wavelength dependence of Rayleigh scattering, which leads to more successive reflections between the surface and the atmosphere with shortening wavelength. Atmospheric reflectance is maximal at 320 nm (Lenoble, 1998). Therefore, it should be expected that the albedo effect decreases with decreasing wavelengths in the UVB, because of ozone absorption of the backscattered photons (Schwander et al., 1999). However, the absence of tropospheric ozone leads to an increase in atmospheric reflectance for decreasing wavelength (Lenoble, 1998). For an Antarctic site, tropospheric ozone can be expected to be well below the global average (IPCC, 2001). Therefore, an increase in the albedo effect for decreasing wavelengths, even in the UVB as seen in Fig. 9, is explained.

Visible. The deviation from unity is less than 20% for all VZA and wavelengths. At 800 nm both ratios deviate from unity by less than 5% for all VZA. At 695 nm and an SZA of 82°, the ratio of grass/snow is even larger than unity by about 5%. This indicates an enhanced horizon brightening for a grass surface. This is in contradiction with the results derived from the luminance measurements shown in Fig. 4. The dependence of radiance on VZA is hardly influenced by different types of surface albedo. Another reason for the weak dependence of the albedo effect for visible wavelengths is that atmospheric scattering is negligible (Lenoble, 1993).

3.3 Radiance vs. luminance

To better compare the measured luminance and the modelled radiance, zenithal scans of radiance for a grass and snow surface are modelled for 550 nm. This is the wavelength where luminance is most effective (see Fig. 1). In this model calculation the default aerosol distribution in the libRadtran package has been used. The default aerosol distribution contains the following parameters (Mayer and Kylling, 2005):

- aerosol_vulcan 1: Aerosol situation above 2 km. 1 means background aerosols.
- aerosol_haze 6: Aerosol type in the lower 2 km of the atmosphere. See E.P. Shettle, ''Models of aerosols, clouds and precipitation for atmospheric propagation studies'', in ''Atmospheric propagation in the UV, visible, IR and mm-region and related system aspects'', AGARD Conference Proceedings (454), 1989. 6 means tropospheric type aerosols.
- aerosol_season 1: Specific season to get appropriate aerosol profile. 1 means spring-summer profile.
- aerosol_visibility 50.0: Visibility in km. Thus, 50 km of horizontal visibility have been used as model input.
- aerosol_tau_file: File containing a profile of aerosol optical depth. In this study the example aerosol_tau_file contained in the libRadtan package has been used. This file contains the aerosol optical depth profile from Eltermann (1968).

In contrast to all other model calculations performed in this study, it has been decided to include aerosols in this case because even a low aerosol content affects the spacial distribution of radiance across the sky. Especially for large VZA, the radiance can be reduced by more than 80% when the default aerosol setting in the model is used. Unfortunately, the true aerosol content for Neumayer during the time of investigation is not available. Figure 10 shows that horizon brightening is most pronounced at a SZA of 48° and a snow covered surface. The ratio of zenithal scans at a particular SZA (lower panel Fig. 10) agrees qualitatively with the measured ratio of luminance zenithal scans (see Fig. 4).

The only investigations of radiance over a snow covered surface reported in the scientific literature have been conducted by Huber et al. (2004). They compared radiance measurements over an inhomogeneously snow covered surface (albedo = 0.4) with model results corresponding to a situation with homogeneously snow covered ground (albedo = 0.8). For a SZA of 45°, they observe an enhancement in radiance of 40% at a VZA of 80° due to the snow covered surface at 310 and 350 nm. The corresponding enhancement

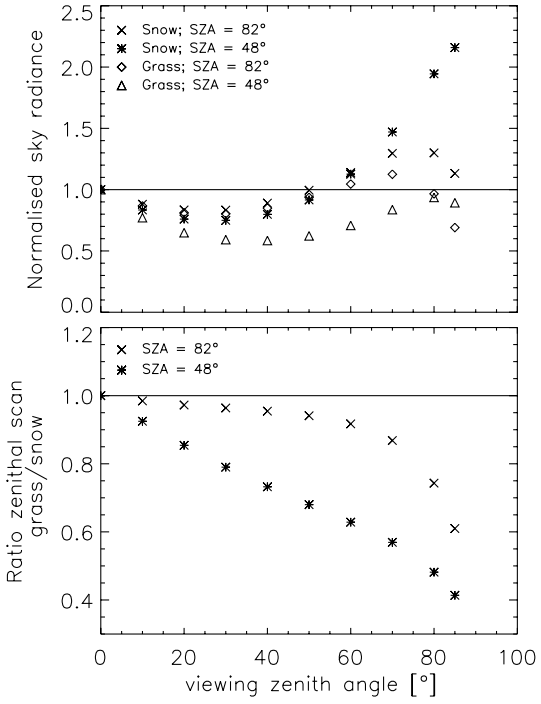

Fig. 10. Modelled zenithal radiance scans for a SZA of 82° and 48° over a grass and snow surface for 550 nm (upper panel). Horizon brightening is most pronounced at a SZA of 48° and a snow surface. Enhanced horizon brightening is observed for snow at both SZA (lower panel). This is in qualitative agreement with the measured luminance distribution (see Fig. 4)

shown in Fig. 9 is only 12% (SZA = 48°, VZA = 80°, $\lambda = 350$ nm), even though the difference between grass and snow albedo equals 0.948 (see Table 1). A reason for the discrepancy between both investigations could be due to the different altitude in which both experiments have been conducted. However, it shows the complexity of this problem and presents the need for additional experimental and modelling studies in order to investigate the effect of varying albedo on spectral radiance.

Another discrepancy arises from the modelling results of the zenithal radiance scans when compared to the experimentally determined zenithal luminance scans. The result of the zenithal luminance scans indicated that horizon brightening increased due to the highly reflective snow surface. This cannot be observed for all of the visible wavelengths in Fig. 9. However, as the three zenithal radiance scans in the visible wavelengths do not behave much differently from each other, completely different behaviour for a modelled radiance scan at 550 nm is not expected, this is supported by Fig. 10. However, Fig. 10 shows a slightly different behaviour of the zenithal scan, with greater dependence on VZA than on measurement (see Fig. 4). This is due to the implementation of aerosols in the model calculations. Without this implementation of aerosols, the modelled radiance at 550 nm would resemble the modelled radiance at 499 nm. This has been tested, however, no complete sensitivity study concerning the influence of aerosols has been performed. Such a study would provide valuable information for future investigations. Thus, aerosols are an important influencing factor when investigating sky radiance distributions. In the next section, the relation of modelled to measured radiance is discussed. An extensive discrepancy between model and measurement is seen for the visible (see Fig. 11), so that the model performance for these wavelengths is debatable and should be viewed with care.

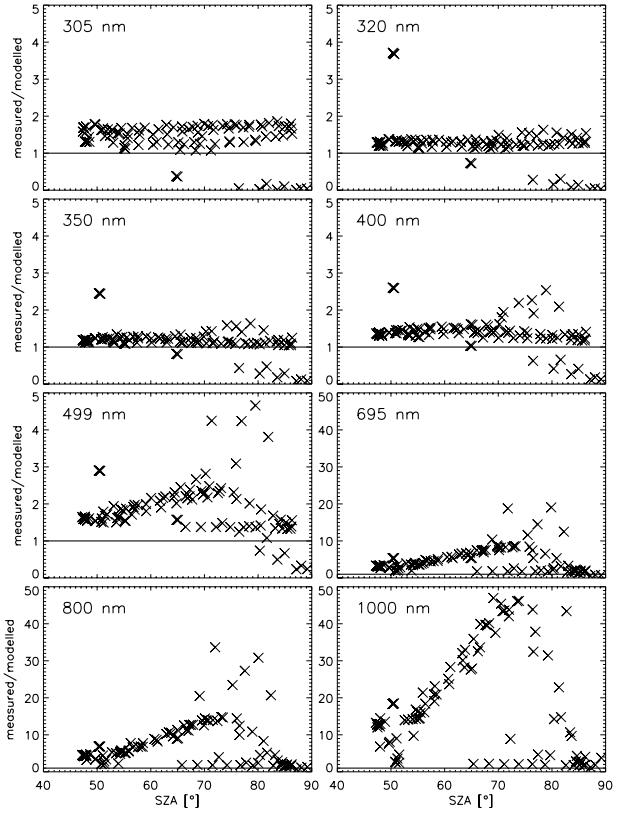

Fig. 11. Ratio of measured to modelled radiance as a function of SZA for all cloudless situations. The ratio is shown for different wavelengths. For wavelengths longer than 400 nm the ratio is very large with values up to 47 for SZA of 75°. At 320 and 350 nm it is minimal with values around 1.2

3.4 Model vs. measurement

All cloud free radiance spectra have been modelled with UVSPEC, a radiative transfer model contained in the libRadtran package (Mayer and Kylling, 2005), which is freely available at *http://www.libradtran.org*. The ratio between modelled and measured radiance as a function of SZA is shown in Fig. 11 for selected wavelengths. The measured radiance mostly exceeds the radiance resulting from model calculations. The deviation between measurement and model is lowest at 320 and 350 nm with an average ratio of 1.2. For wavelengths longer than 400 nm a dependence of the ratio on SZA can be seen. The ratio increases for increasing SZA up to 75°, then decreases again steeply until values of 1.2 are reached. For a few cases, the ratios stay around 1.3 for all SZA. A few outliers can also be observed. One is, for example, at a SZA of 50° at 320 and 350 nm. The various sources of these deviations are found in both, the measured absolute spectral radiance and the model calculations.

3.4.1 Absolute radiance calibration

The absolute calibration of radiance as described in Section 2.2.1 involves uncertainties that can partly be eliminated by improving the calibration procedure in future. The main shortcoming is that no calibrated reflectance plaque had been available. By measuring the calibration lamp directly, only part of the input optics is illuminated by the lamp. In the case of an inhomogeneous optical fibre bundle, the entrance slit of the monochromator is not evenly illuminated. This can be achieved by a diffuse radiation source such as a calibrated reflectance plaque. Radiance calibrations employing such a reflectance reference are described by Mueller et al. (2003) or Meister et al. (2003). Diffuse illumination of the entrance optics for radiance measurements is important as the sky light also illuminates the entrance optics in a diffuse way.

3.4.2 Performance of the cylindrical input optics

It is assumed that incident light originating from about 70° to 75° from the 0° direction is reflected inside the input cylinder. This deficiency is supported by various factors. However, measurements taken from an angular distance of 70° to 75° between the input optics and the sun are excluded from the data analysis. This is one of the reasons why the useful data set is rather small. This malfunction of the radiance input optics has been detected during the Antarctic campaign and verified afterwards in the laboratory.

Design of the input optics. Reflections of light inside the input tubus are possible because it is not manufactured with a black coating on the inside of the cyclinder. The specifications of the input cylinder did not yield any malfunction. It is comparably short (10 cm) and has a wide FOV (4.4°). In contrast, the input cylinder deployed by Blumthaler et al. (1996) and Huber et al. (2004) is 30 cm long and has a FOV of only 1.5°.

FOV measurement. The FOV of the input optics has been measured by turning the cylindrical input optics in steps of 0.5° up to ±5° from the centre. The centre is denoted the direction of normal incidence. To investigate possible problems of reflected light inside the input cylinder the input optics has been measured in steps of 5° from ±90°. These measurements indicate local maxima at ±70° from the centre. These are by one order of magnitude larger than the values at angles of about 10° to 60° from the centre and by four orders of magnitude lower than the maximum at 0°. Diffuse sky radiance is typically four to five orders of magnitude below the direct irradiance of the sun (Gröbner, 1996). Thus, the depression of reflected light may not be sufficient.

Diurnal cycle of zenith radiance. The diurnal cycle of zenith radiance (see Fig. 6) shows local maxima at 06:00 as well as 18:30 UTC for wavelengths larger than 499 nm. A detector based problem can be excluded as at 499 nm the photomultiplier is active, whereas the silicon diode is addressed for wavelengths longer than 500 nm. So, both detectors show these local maxima. The SZA at 06:00 and at 18:30 UTC is 70.5° and 68.6°, respectively, which would support the assumption of detecting reflected direct sun light inside the input cylinder.

Comparison with diurnal cycle of luminance. The diurnal cycle of luminance (see Fig. 3) does not show these local maxima at SZA of about 70°. Therefore, these maxima have to be based on a malfunction of the cylindrical input optics.

For these reasons the maximum deviations between measurement and model are found when

the angle between the position of the input cylinder and the sun is between 70° to 75°. As most radiance measurements are performed for the zenith, the SZA describes this angle of difference. Thus, the maximal deviations in Fig. 11 are observed at a SZA of 75°. This feature is stronger with increasing wavelength because the direct component of the incident irradiance is larger with increasing wavelength (Seckmeyer, 1997). Since not all radiance measurements have been performed for the zenith direction, a few ratios between model and measurement remain around 1.3, independent of SZA. The measured radiance shown in Fig. 7 is exactly one of these cases where the ratio between measured and modelled radiance only shows this systematic deviation. The zenithal scans shown in Fig. 7 have been recorded with the angular distance between the entrance optics ranging between 82° and 167°. Thus, the sky radiance measurements shown in this analysis are not affected by the deficient input optics. In addition, the large solar zenith angle of 82° implies a low direct component of the incident radiation also minimising the error based on the internal reflections. Due to the stray light problems of the input optics for an angular distance to the sun of about 70° a number of sky radiance measurements could not be considered. Thus, it was only possible to investigate distribution of sky radiance for a limited number of cases. A comprehensive model validation was therefore not possible due to the restricted number of available data, which conveys the need for additional measurements of sky radiance in an Antarctic environment.

3.4.3 Accuracy of input parameters

Total ozone column. The deviation between measured and modelled radiance at 305 nm is larger compared to wavelengths in the UVA. This is because the total ozone column was not adequately known. TOMS data were used as input parameter. However, TOMS is known to overestimate total column ozone for Antarctic sites by 4 to 10% (Bernhard et al., 2002). Thus, too much radiation is absorbed leading to lower radiance values. Decreasing the ozone column would lead to a reduction in the modelled radiance, and thus, to a smaller deviation between model and measurement at 305 nm. Particularly for SZA larger than 80°, the TOMS data should be used carefully according to McPeters and Labow (1996). Despite these concerns, TOMS data have been used because they provide a complete data set for the days that have been modelled.

Aerosols. Aerosols have not been included in the model as aerosol information was not available. However, the assumption of zero aerosols is justified as the Antarctic atmosphere is known to be very clean (Piel, 2004). At the South Pole, Bernhard et al. (2004) also did not include any aerosols for radiative transfer calculations in the UV region. The exception is the modelled radiance scan at 550 nm (see Fig. 10), where a default aerosol distribution has been implemented in the radiative transfer calculations. Aerosols alter the spatial distribution of radiance across the sky. Especially for large VZA, aerosols can reduce the absolute radiance by more than 80% compared to the aerosol free case. Thus, ancillary aerosol information would be valuable for exact modelling of the radiative transfer.

Polarisation. Polarisation has also not been accounted for. Radiance is not evenly polarised across the sky (Huber et al., 2004; Lenoble, 2004; Liu and Voss, 1997). When neglecting polarisation in radiative transfer calculations, the error varies approximately between -8% and $+8\%$. The error is negative on the side of the sun (neglecting polarisation underestimates the radiance), and positive (overestimation) on the opposite side (Lenoble, 2004). However, the error decreases with increasing surface albedo (Mishchenko et al., 1994). As radiance has mostly been measured opposite the sun, the modelled radiance overestimates the true value. Including polarisation would decrease the model result leading to a better agreement between measured and modelled radiance. The response of the IMUK spectroradiometer with the input cylinder as entrance optics is not dependent on the polarisation of the incoming radiation. This was tested in the IMUK radiation laboratory by placing a linear polarising filter between the entrance optics and a 100 W calibration lamp. The filter was turned in steps of 45°. The response of the IMUK spectroradiometer only changed within $\pm 1\%$ for all wavelengths between 250 and 1000 nm, which is the achievable accuracy when repeating measurements of a 100 W calibration lamp. Thus, the measured absolute radiance is

not dependent on the degree of polarisation of the sky radiance. Only the model results convey an uncertainty based on polarisation.

Atmospheric profiles. The atmospheric profiles used to model radiance have been provided in the libRadtran package. They refer to a subarctic summer situation. Antarctic profiles have not been used because they are not contained in the standard version of libRadtran. Bernhard et al. (2002) remark that, in particular, the ozone and temperature profiles used in the model have an important influence on its performance, especially for large SZA. The spectral regions where the largest deviations are found are not affected very much by the ozone profile.

3.4.4 Model performance

To our knowledge there is no peer reviewed literature stating that UVSPEC has been validated for radiance in the complete wavelength range. However, the comparison between UVSPEC and results from a successive orders of scattering (SOS) radiative transfer code, kindly provided by Prof. Jacqueline Lenoble, Université Joseph-Fourier, Grenoble, France, indicates that the performance of both models seems to be satisfactory in the UV. Both models have been evaluated in a model intercomparison for spectral irradiance performed by van Weele et al. (2000). Deviations of up to 20% occur at 305 nm. They may be due to mid-latitude atmospheric profiles used in the SOS code. However, the few model ratios that have been calculated for zenith radiance are too sparse to draw a final conclusion.

The visible and near infrared up to 1050 nm is the spectral region with the largest deviations between model and measurement. For wavelengths larger than 500 nm, molecular absorption in the atmosphere has to be considered. In this study, the absorption parameterisation according to Ricchiazzi et al. (1998) has been employed. This parameterisation is certainly not as accurate as, for example, line-by-line calculations (Edwards, 1992). For SZA $< 80^\circ$ a spherical approximation to solve the radiative transfer equation has been applied in the model calculations (see Section 3.2.2).

For a proper validation of the model, the input parameters would have to be known with greater accuracy. Furthermore, a wide range of atmospheric conditions needs to be considered to test the model with the largest possible combination of input parameters. Only this way, can statistically significant results be obtained.

4. Conclusions

Zenith luminance for overcast situations can be larger by one order of magnitude compared to cloudless situations. The maximum luminance occurs during cloud free situations in the aureole. For cloudless situations, in contrast to overcast skies, horizon brightening is observed. Over a snow covered surface, at a viewing zenith angle of 84°, the luminance exceeds the zenith luminance by a factor of 8.2 and 7.6 for a solar zenith angle of 86° and 48°, respectively. Over a surface covered by grass this factor only amounts to 4.9 for a solar zenith angle of 86°. Horizon brightening over grass for a solar zenith angle of 48° is hardly noticeable, with the luminance at a viewing zenith angle of 84° being only 1.4 times larger than the zenith luminance. Under a sky with stratiform cloud cover, horizon brightening is not observed at all in this study. The reason for the horizon brightening can be explained by scattering processes in the atmosphere. Horizon brightening is enhanced over a snow covered surface (high albedo) compared to grass (low albedo). At a viewing zenith angle of 84° this enhancement amounts to a factor of 5 and 1.7 for solar zenith angles of 48° and 86°, respectively.

Spectral radiance measurements show the radiance distribution over the sky becomes less homogeneous with larger wavelengths. This is also confirmed by model results. At 305 nm, the radiance at the horizon is only about 80% of the zenith radiance. At 1000 nm, the measured radiance opposite the position of the sun exceeds the zenith radiance by a factor of 11.

Model calculations of spectral radiance show that an enhancement of horizon brightening due to a snow covered surface cannot be seen for 695 and 800 nm. For most situations, horizon brightening is more pronounced the shorter the wavelength. At a solar zenith angle of 82°, the enhancement in radiance close to the horizon due to a high compared to a low surface albedo is 73% and only 16% at 305 and 499 nm, respectively. All results are derived from measurements where the solar zenith angle and the viewing zenith angle of the input optics differ by more than 80° to avoid the angular regions around 70°

where direct reflections inside the cylindrical input tubus affect the measured radiance. The radiative transfer model has, so far, has not been comprehensively validated for irradiance in the visible and infrared spectral region nor for spectral radiance from 280 to 1050 nm. Thus, more systematic investigations and/or new model developments are needed before confirmed conclusions from model studies can be drawn for spectral radiances under polar conditions.

Radiative transfer calculations of radiance at 550 nm show qualitatively the same behaviour as measured luminance distributions. These were the only model calculations with aerosols included.

The luminance measurements complement the radiance measurements based on the difference in acquisition. The advantage of the luminance measurements is the fast coverage of the complete sky in about 40 seconds. Spectral information can only be obtained from radiance measurements. Thus, it is a favourable strategy to decide upon the direction and atmospheric situations of radiance measurements after the distribution of luminance has been observed.

In this Antarctic campaign, only limited atmospheric situations have been considered. Despite these limitations it can be concluded that a change in albedo conditions, which is predicted as a consequence of climate change (IPCC, 2001), will significantly change the radiation conditions in polar regions.

Acknowledgements

This study was funded by the *Deutsche Forschungsgemeinschaft* (*DFG*) within the context of the *Schwerpunktprogramm Antarktisforschung*. The instrumentation was jointly sponsored by the DFG and the state of Lower Saxony in Germany. Logistic support for the Antarctic measurements has been provided by the Alfred Wegener Institute Bremerhaven, Foundation for Polar and Marine Research, Germany.

References

Bais AF, Gardiner BG, Slaper H, Blumthaler M, Bernhard G, McKenzie R, Webb AR, Seckmeyer G, Kjeldstad B, Koskela T, Gröbner J, Kerr JB, Kazadsis S, Leszczynski K, Wardle D, Brogniez C, Josefsson C, Gillotay D, Reinen H, Weihs P, Svenoe T, Eriksen P, Kuik F, Redondas A (2001) The SUSPEN intercomparison of ultraviolet spectroradiometers. J Geophys Res 106: 12509–12526

Bernhard G, Seckmeyer G (1997) New entrance optics for solar spectral UV measurements. Photochem Photobiol 65: 923–930

Bernhard G, Seckmeyer G (1999) Uncertainty of measurements of spectral solar UV irradiance. J Geophys Res 104: 14321–14345

Bernhard G, Booth C, Ehramjian J (2002) Comparison of measured and modelled spectral ultraviolet irradiance at Antarctic stations used to determine biases in total ozone data from various sources. In: Slusser J, Herman J, Gao W (eds) Ultraviolet ground and space-based measurements, models and effects. Vol. 4482 of Proceedings of SPIE, Bellingham, Washington, D.C., pp 115–126

Bernhard G, Booth C, Ehramjian J (2004) Version 2 data of the National Science Foundations Ultraviolet Radiation Monitoring Network: South Pole. J Geophys Res 109: doi:10.1029/2004JD004937

Blumthaler M, Gröbner J, Huber M, Ambach W (1996) Measuring spectral and spatial variations of UVA and UVB sky radiance. Geophys Res Lett 23: 547–550

Dahlback A, Stamnes K (1991) A new spherical model for computing the radiation field available for photolysis and heating at twilight. Planet Space Sci 39: 671–683

DIN 5031 (1982) Strahlungsphysik im optischen Bereich und Lichttechnik. Beuth Verlag, 8 pp

Edwards DP (1992) GENLN2: A general line-by-line atmospheric transmittance and radiance model: Version 3.0 description and users guide, Tech. Rep. NCAR/TN-367 + STR, National Center for Atmospheric Research (NCAR), Boulder, Colorado

Eltermann K-U (1968) UV, visible and IR attenuation for altitudes to 50 km, Tech. Rep. AFCRL-68-0153, Air Force Cambridge Research Laboratories, Bedford, MA, USA

Feister U, Grewe R (1995) Spectral Albedo Measurements in the UV and visible region over different types of surfaces. Photochem Photobiol 62: 736–744

Grant R, Heisler G (1997) Obscured overcast sky radiance distributions for ultraviolet and photosynthetically active radiation. J Appl Meteor 36: 1337–1345

Grant R, Heisler G, Gao W (1997a) Clear sky radiance distributions in ultraviolet wavelength bands. Theor Appl Climatol 56: 123–135

Grant R, Heisler G, Gao W (1997b) Ultraviolet sky radiance distributions of translucent overcast skies. Theor Appl Climatol 58: 129–139

Gröbner J (1996) Ultraviolet solar radiance measurements using a high precision spectroradiometer. PhD Thesis, Naturwissenschaftliche Fakultät der Leoplold-Franzens-Universität Innsbruck, Innsbruck, Austria: 101 pp

Huber M, Blumthaler M, Schreder J, Schallhart B, Lenoble J (2004) Effect of inhonogeneous surface albedo on diffuse UV sky radiance at a highaltitude site. J Geophys Res 109: doi:10.1029/2003JD004013

Karsten U, Bischof K, Hanelt D, Wiencke D (1999) The effect of ultraviolet radiation on photosynthesis an ultraviolet-absorbing substances in the endemic Arctic macroalga Devaleraea ramentacea (Rhodophyta). Physiologia Plantarum 105: 58–66

Kiedron PW, Michalsky JJ, Berndt JL, Harrison LC (1999) Comparison of spectral irradiance standards used to calibrate shortwave radiometers and spectroradiometers. Appl Opt 38: 2432–2439

Kurudz R (1992) Synthetic infrared spectra. In: Proceedings of the 154th Symposium of the International Astronomical

Union (IAU), Tuscon, Arizona. Kluwer, Acad., Norwell, MA, 1365–1368

Kylling A, Dahlback A, Mayer B (2000) The effect of clouds and surface albedo on UV irradiances at a high latitude site. Geophys Res Lett 27: 1411–1414

Lenoble J (1993) Atmospheric radiative transfer. Hampton, VA: A. Deepak Publishing, 532 pp

Lenoble J (1998) Modelling of the influence of snow reflectance on ultraviolet irradiance for cloudless sky. Appl Opt 37: 2441–2447

Lenoble J (2004) Importance of polaristion in calculations of radiance and irradiance. In: Seckmeyer G, Martin T, Ali T (eds) European database for UV climatology and evaluation. Final report to the commission of the European communities, contract No. EVK2-CT-199900028, 100 pp

Liu Y, Voss K (1997) Polarized radiance distribution measurements of skylight. II. Experiment and data. Appl Opt 36: 8753–8764

Mayer B, Seckmeyer G, Kylling A (1997) Systematic long-term comparison of spectral UV measurements and UVSPEC modelling results. J Geophys Res 102: 8755–8767

Mayer B, Kylling A (2005) Technical note: The libRadtran software package for radiative transfer calculations description and examples of use. Atmos Chem Phys Discuss 5: 1319–1381

McPeters RD, Labow GJ (1996) An assessment of the accuracy of 14.5 years of Nimbus 7 TOMS Version 7 ozone data by comparison with the Dobson network. Geophys Res Lett 23: 3695–3698

Meister G, Abel p, Carder K, Chapin A, Clark D, Cooper J, Davis C, English D, Fargion G, Feinholz M, Frouin R, Hoge F, Korwan D, Lanzin G, McClain C, McLean S, Menzies D, Poteau A, Robertson J, Sherman J, Voss K, Yungel J (2003) The Second SIMBIOS Radiometric Intercomparison (SIMRIC-2), March–November 2002, report NASA/TM-2003, Greenbelt, Maryland: Goddard Space Flight Center, 65 pp

Mishchenko MI, Lacis AA, Travis LD (1994) Errors induced by the neglect of polarization in radiance calculations for Rayleigh-scattering atmospheres. J Quant Spectrosc Radiat Transfer 51: 491–510

Mueller J, Pietras C, Hooker S, Austin R, Miller M, Knobelspiesse K, Fouin R, Holben B, Voss K (2003) Instrument specifications, characterization and calibration, ocean optics protocols for satellite ocean color sensor validation revision 4, Volume II. Greenbelt, Maryland: Goddard Space Flight Center, 57 pp

Nichol S, Pfister G, Bodeker G, McKenzie R, Vood S, Bernhard G (2003) Moderation of cloud reduction of UV in the Antarctic due to high surface albedo. J Appl Meteor 42: 1174–1183

Piel C (2004) Variability of chemical and physical parameters of aerosol in the Antarctic troposphere. Reports on Polar and Marine Research 476. Bremerhaven, Germany: Alfred Wegener Institute for Polar and Marine Research, 157 pp

Prather M, Ehhalt D, Dentener F, Derwent R, Dlugokencky E, Holland E, Isaksen I, Katima J, Kirchhoff V, Mathson P, Midgley P, Wang M (2001) Atmosperic chemistry and greenhouse gases in climate change 2001: The scientific basis. Contribution of Working Group I to the Third Assessment Report of the Intergovernmental Panel on Climate Change. Cambridge, United Kingdom and New York, NY, USA: Cambridge University Press, pp 239–287

Ricchiazzi P, Young S, Gautier C, Sowle D (1998) A research and teaching software tool for plane-parallel radiative transfer in the Earths atmosphere. Bull Amer Meteor Soc 79: 2101–2114

Schwander H, Mayer B, Ruggaber A, Albold A, Seckmeyer G, Köpke P (1999) Method to determine snow albedo values in the UV for radiative transfer modelling. Appl Opt 38: 3869–3875

Seckmeyer G (1997) Die genaue Messung und Simulation der solaren UV-Strahlung, Habilitationsschrift, Technische Universität Ilmenau, 116 pp

Seckmeyer G, Bais A, Bernhard G, Blumthaler M, Eriksen P, McKenzie RL, Roy C, Miyauchi M (2001) Instruments to measure solar ultraviolet radiation, part I: spectral instruments. WMOGAW report 126, 30 pp

Stamnes K, Tsay SC, Wiscombe W, Jayaweera K (1988) Numerically stable algorithm for discreteordinate-method radiative transfer in multiple scattering and emitting layered media. Appl Opt 27: 2502–2509

Takao T, Aono M, Kishi T, Sakurai K, Ijima O, Takawa M, Narita O, Shitamichi M (1999) Ultraviolet spectral irradiance observations at Syowa Station, Antarctica 1991–1996. The Geophysical Magazine Series 2: 95–107

Tregenza P (1987) Subdivision of the sky hemisphere for luminance measurements. Lightning Research and Technologies 19: 13–14

van Weele M, Martin TJ, Blumthaler M, Brogniez C, den Outer PN, Engelsen O, Lenoble J, Mayer B, Pfister G, Ruggaber A, Walravens B, Weihs P, Gardiner BG, Gillotay D, Haferl D, Kylling A, Seckmeyer G, Wauben WMF (2000) From model intercomparison toward benchmark UV spectra for six real atmospheric cases. J Geophys Res 105: 4915–4925

Weihs P, Webb A, Hutchinson S, Middelton G (2000) Measurements of the diffuse UV sky radiance during broken cloud conditions. J Geophys Res 105: 4937–4944

Wuttke S, Benhard G, Ehramjian J, McKenzie R, Johnston P, ONeill M, Seckmeyer G (2005) New spectroradiometers complying with the NDSC standards. J Atmos Oceanic Technol (in press)

Wuttke S, Seckmeyer G, König-Langlo G (2005a) Measurements of spectral snow albedo at Neumayer, Antarctica. Annales Geophysicae (accepted)

Authors' addresses: S. Wuttke (e-mail: swuttke@awi-bremerhaven.de), Institute for Polar and Marine Research, Am Handelshafen 12, 27570 Bremerhaven, Germany; G. Seckmeyer, Institute of Meteorology and Climatology, University of Hannover, Herrenhäuser Strasse 2, 30419 Hannover, Germany.